

Optimization of nanostructured permalloy electrodes for a lateral hybrid spin-valve structure

T. Last,* S. Hacia, M. Wahle, S.F. Fischer,[†] and U. Kunze
Werkstoffe und Nanoelektronik, Ruhr-Universität Bochum, 44780 Bochum, Germany
(Dated: February 8, 2020)

By means of room temperature magnetic force microscopy at remanence an optimized geometry for highly remanent permalloy (Py) electrodes in a lateral ferromagnet-semiconductor-ferromagnet device structure is presented. The multidomain to single-domain transition for rectangular Py micro- and nanostructures is mapped and compared with a phenomenological model. Py structures with low aspect ratios $m \lesssim 3$ form up in few well known multidomain patterns. For medium aspect ratios from $m \approx 4$ to $m \approx 20$ highly remanent states with closure domains originate. We classify $m \gtrsim 20$ as the high aspect ratio regime with Py wires being in a single-domain state. Introducing lateral kinks in the Py wire disturbs the highly remanent domain state. However, domain wall pinning at vertical flanks leads to a uniform magnetized state at the ferromagnet-semiconductor contact.

PACS numbers: 75.75.+a, 75.60.-d, 75.47.-m, 85.75.-d

I. INTRODUCTION

Lateral nanoscale ferromagnet-semiconductor (FM-SC) devices have attracted much interest recently for future spintronics applications [1, 2, 3, 4]. Beside the tailor-made SC substrates a profound knowledge of the magnetic properties of the FM electrodes required as spin-polarizer and -analyzer is essential [5]. Low aspect ratio permalloy (Py) electrodes (aspect ratios $m = 1, 2$) had been examined by G. Meier, *et al.* [6]. The multidomain configuration of low aspect ratio Py structures leads to a reduction of the stray field. However, an application for zero-field operation is limited as a maximum degree of spin-polarization cannot be achieved by a multidomain configuration. Furthermore, for Py platelets with $m = 2$ a variety of different metastable remanent magnetic states can be found [7], although a well defined remanent domain state is favourable [1]. Here, we present the optimization of the domain configuration of rectangular permalloy (Py) micro- and nanostructures which are used as electrodes for low-field operation in a lateral hybrid device geometry by means of room temperature magnetic force microscopy (MFM) at remanence. We show that high aspect ratio Py electrodes have two major advantages: they show a single-domain behaviour at the FM-SC contact due to intentionally introduced pinning centres for domain walls such as vertical flanks and allow lateral kinks outside the contact area. Lateral kinks are of importance as they are introduced in hybrid devices in order to bridge the gap between the nanoscale electrodes and microscale bond pads. Our MFM study comprises three steps. First, we map the multidomain to single-domain transition for rectangular permalloy (Py, Ni₈₀Fe₂₀) micro- and nanostructures. The results are compared with calculations based on a theoretical model

developed by A. Aharoni [8] for prolate spheroids and experimental data for Py (R.D. Gomez, *et al.* [13]) and Co (E. Seynaeve, *et al.* [9]). Second, magnetic field supported MFM is used to study the switching from parallel to antiparallel magnetization alignment of adjacent Py wires of varying widths [4, 10], as a controlled switching behaviour is of vital importance for spin-valve operation. Third, the influence of lateral kinks and vertical flanks on the formation of domain walls is studied for a lateral Py-InAs spin-valve structure.

II. PREPARATION AND EXPERIMENT

In order to map the multi- to single-domain transition rectangular polycrystalline Py micro- and nanostructures are prepared on p-Si (111) and undoped n-type InAs (100) by high-resolution electron-beam lithography (EBL), electron-beam evaporation (EV) and lift-off. Lengths l and widths w of the ferromagnetic structures are varied from 200 nm both up to 60 μm and up to 30 μm , respectively, covering aspect ratios $m = l/w$ from 1 to 105. The fabrication of an InAs-based lateral spin-valve structure which is shown in Fig. 1 comprises the following steps. InAs is chosen because of its strong spin-orbit interaction which makes it a promising candidate for the semiconductor in a spin field-effect transistor [1, 11, 12]. On the InAs substrate a 200 nm thick SiO₂

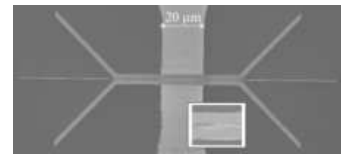


FIG. 1: Scanning electron microscope image of a lateral Py-InAs spin-valve structure with electrodes of widths 2 μm and 0.4 μm separated by 0.2 μm in the contact area. Inset: Enlargement of the Py electrodes.

*Electronic mail:thorsten.last@rub.de

[†]Electronic mail:saskia.fischer@rub.de

film is sputtered and laterally structured by means of optical lithography and wet chemical etching to implement a $20\ \mu\text{m}$ broad contact area to the semiconductor. Thereafter a tunnelling oxide is thermally grown on the InAs in the contact area at $T = 140\ ^\circ\text{C}$ in dry O_2 for 120 min. The electrodes ($w = 2\ \mu\text{m}$, $0.4\ \mu\text{m}$; separation $s = 0.2\ \mu\text{m}$) are prepared by patterning a 80 nm PMMA (polymethylmethacrylate) film using EBL at 5 kV, EV and lift-off in acetone (thickness $t = 38\ \text{nm}$ and 50 nm). MFM is performed with a Nanoscope MultiMode SPM (DI) operating in the TappingMode/LiftModeTM. A commercially available probe (MESP, DI) is used and premagnetized along its vertical direction. Lift scan heights of about 120 nm are applied to minimize the probe induced perturbations.

III. RESULTS AND DISCUSSION

A. Multidomain to single-domain transition

For Py films the magnetocrystalline anisotropy is negligible at room temperature and the resulting magnetization arrangement is determined by the competition between the exchange energy and the stray field energy. It is therefore possible to tune the remanent domain configuration of a rectangular thin film Py structure by varying its aspect ratio. In Fig. 2 a MFM image of a matrix of Py microstructures having lengths and widths from $1\ \mu\text{m}$ to $10\ \mu\text{m}$ is shown. Around the diagonal microstructures

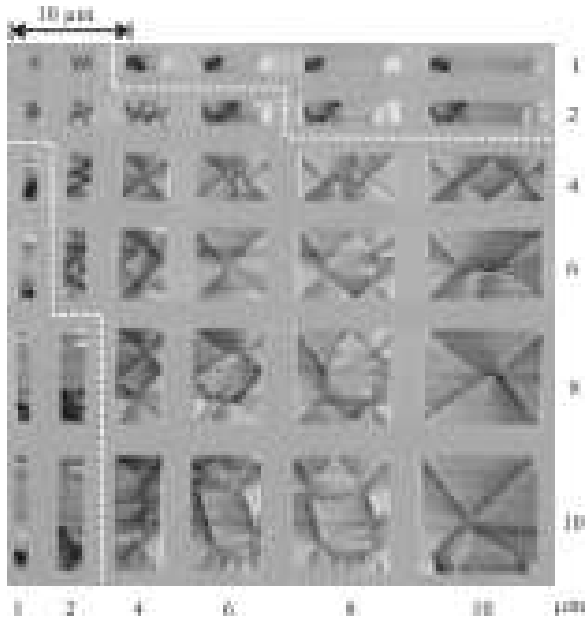


FIG. 2: Magnetic force microscope image of a matrix of Py structures in remanence with low and medium aspect ratios m ranging from 1 (diagonal) to 10 (bottom left and top right). The lateral dimensions are indicated for the columns and rows beside the image. Dashed white lines indicate the transition from low to medium aspect ratio structures.

with low aspect ratios from 1 to 3 resulting in five principle multidomain patterns [13, 14, 15]: (i) four closure domains with four 90° walls (fan figure), (ii) four closure domains with four 90° walls and one 180° wall, (iii) four closure domains with four 90° walls and one 180° wall with cross-tie inclusions, (iv) seven closure domains (tilted diamond figure) and (v) seven closure domains with cross-tie inclusion. In Fig. 2, type (i) is formed in most squared structures ($m = 1$), except for (8,8) with a type (v) domain configuration. The type (i) pattern can also be found in slightly non-squared structures (10,8), where the singular point where the four domain walls meet is displaced out of the centre of the structure. Microstructures with $m = 1.25$ and 1.33 prefer to be in the type (v) pattern. Type (ii), (iii) and (iv) domain configuration are favorable in Py structures with aspect ratios from 1.5 to 2.5. The region around $m = 3$ can be denoted as a transition region (structures (2,6) and (6,2)) from multidomain states to highly remanent states and from $m = 4$ on only highly remanent states originate. Such patterns can be seen in the upper right and lower left part of the MFM image. These highly remanent states consist of a featureless central region which indicates a uniform magnetization parallel to the length of the microstructures and fan-type closure domains at both ends. The pronounced closure domains diminish and the region of homogeneous magnetization is increasing with decreasing structure width. This evolution can clearly be seen in Fig. 3 (a) where a MFM image of an array of nanostructured wires of aspect ratios ranging from 14.2 to 32.7 is shown ($l = 20.9\ \mu\text{m}$, $w = 1.47\ \mu\text{m}$ to $0.64\ \mu\text{m}$ (wire 1-8); $l = 16.7\ \mu\text{m}$, $w = 0.53\ \mu\text{m}$ (wire 9)). For

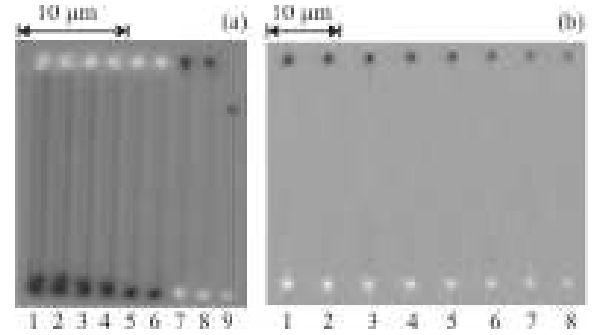


FIG. 3: Magnetic force microscopy images of permalloy nanowire arrays in remanence: (a) $l = 20.9\ \mu\text{m}$, $w = 1.47\ \mu\text{m}$ (wire Nr. 1) to $0.64\ \mu\text{m}$ (Nr. 8); $l = 16.7\ \mu\text{m}$, $w = 0.53\ \mu\text{m}$ (Nr. 9); the aspect ratio varies from 14.2 to 32.7; (b) $l = 32.5\ \mu\text{m}$, $w = 1.11\ \mu\text{m}$ (Nr. 1) to $0.57\ \mu\text{m}$ (Nr. 9); the aspect ratio varies from 29.2 to 57.

aspect ratios greater than 20 the closure domains are no longer visible and longitudinal stray fields are depicted by single colour code (black and white). Single-domain behaviour of the nanowires is more pronounced in Fig. 3 (b) with increased aspect ratio of the wires from 29.2 up to 57.0 ($l = 32.5\ \mu\text{m}$, $w = 1.11\ \mu\text{m}$ (wire 1) to $0.57\ \mu\text{m}$ (wire 8)).

The transition from a multi- to a single-domain state is given in Fig. 4, which summarizes the domain patterns for all investigated structure sizes and aspect ratios, and includes a transition line from a phenomenological model developed by A. Aharoni [8]. Below a lower

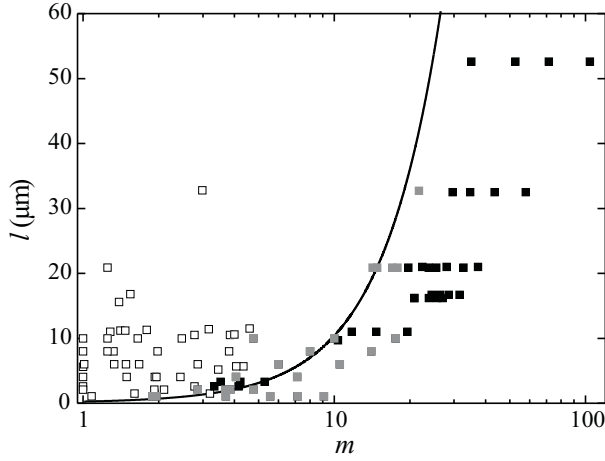


FIG. 4: Diagramm of experimentally observed domain states of Py micro- and nanostructures for varied aspect ratios m versus length l . Open squares indicate a multidomain state, highly remanent states are denoted as black bordered grey squares and closed squares indicate a single-domain state. The black solid line depicts the transition line between multi- and single-domain configuration from a phenomenological model [8].

bound, namely the minor semiaxis a_{c0} , ellipsoidal particles are found to be in a single-domain state in remanence. The lower bound depends on the exchange interaction, on the saturation magnetization and on the aspect ratio m , the aspect ratio between the particle's major and minor axis. According to Seynaeve, *et al.* [9], a critical length $L_c = 2ma_{c0}$ separates the multidomain states (above L_c) from the single-domain states (below L_c). For the calculation the bulk saturation magnetization of Py, 800 kA/m, is taken and an exchange constant of $1.3 \cdot 10^{-9}$ J/m is required, 2 orders of magnitude higher than the reported bulk value of Py [15]. A comparable deviation was found in the analogue evaluation of domain structures for Co microstructures [9]. Several reasons account for this discrepancy. While the model is based on ellipsoidal particles, we investigate rectangular Py microstructures, which changes profoundly the calculation of the stray field. Furthermore, the prepared structures exhibit finite surface and edge roughness due to vapor deposition and lift-off, which introduces magnetization inhomogeneities. Third, MFM data exhibits a resolution limit of the order of the probe lift scan height, which is approximately 120 nm. Nevertheless, the observed transition between a multi- and a single-domain configuration agrees qualitatively with the expected behaviour from [8]. As a consequence high aspect ratios ($m \geq 20$) of Py wires provide a reliable single-domain state in remanence and are advisable for electrodes in a lateral FM-SC device.

B. Width-dependence of switching field

According to micromagnetism the switching field $\mu_0 H_C$ of elongated Py wires is essentially determined by their widths. Here, we demonstrate antiparallel magnetization configuration by magnetic field supported MFM for Py wires of aspect ratios relevant to FM/SC devices. Our magnetotransport studies on comparable single Py wires show that the switching field increases linearly with reciprocal wire width [10]. In Fig. 3, MFM images of an array of nanoscale Py wires are shown after applying a longitudinal magnetic field prior to imaging. In

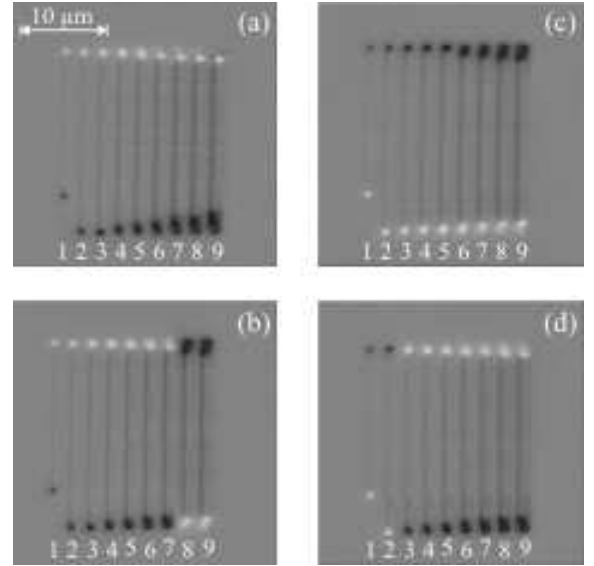


FIG. 5: MFM images of an array of nanoscale Py wires (lengths and widths, see Fig. 3) to illustrate the width-dependent subsequent switching in longitudinal magnetic field. The nanowires are magnetized in an applied magnetic field prior to imaging with (a) +60 mT, (b) -20 mT, (c) -60 mT and (d) +20 mT.

the following, wires depicted as 2 ($w = 0.5 \mu\text{m}$) and 9 ($w = 1.4 \mu\text{m}$) are pointed out to illustrate the width-dependent subsequent switching (Fig. 5 (a)-(d)). After applying a magnetic field of +60 mT all wires are magnetized in parallel direction. In reversed field a change in the magnetization configuration occurs after application of -20 mT, at which the magnetization of the broad wires is switched. At fields of -60 mT all wire magnetization directions are reversed. This subsequent switching occurs as well at a reversed magnetic field sweep from -60 mT to 60 mT. In consequence antiparallel magnetization configuration of wires labelled 2 and 9 in Fig. 3 exists in a field range of 40 mT, feasible for FM-SC devices.

C. Lateral kinks in medium aspect ratio wires

As shown above rectangular Py microstructures with medium aspect ratios $m \geq 4$ are highly remanent. The

perturbation of this domain configuration by introducing horizontal kink angles between 0° and 90° in the centre of short Py wires of widths $w = 2 \mu\text{m}$, length $l = 10 \mu\text{m}$ ($m = 10$) is depicted in Fig. 6. A straight wire (Fig. 6

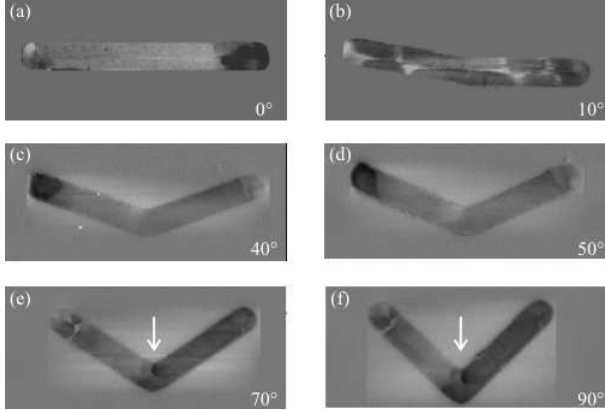


FIG. 6: MFM images of Py wires where horizontal kinks of angles 0° (a), 10° (b), 40° (c), 50° (d), 70° (e) and 90° (f) are introduced in the centre of Py wires of widths $w = 2 \mu\text{m}$, length $l = 10 \mu\text{m}$ ($m = 10$). Arrows in (e) and (f) depict the insertion of domain walls at the lateral kink.

(a)) possesses the expected highly remanent domain configuration with significant closure domains at both ends and a homogeneous magnetized mid-part. However, a 10° kink changes the domain configuration drastically (Fig. 6 (b)). Here, cross-tie walls separate the two main domains. With increasing kink angle the domain configuration transforms back to highly remanent states, but a significant magnetization inhomogeneity at the centre of the structure is observable (Fig. 6 (c), (d)), where from kink angles of 70° to 90° a domain wall generates. Consequently, horizontal kink angles introduced in the Py wire of medium aspect ratio disturb the highly remanent domain state.

D. Lateral kinks and vertical flanks in high aspect ratio wires

Following the above domain investigations we present the electrode geometry of an InAs-based spin-valve structure to study spin-dependent transport. In Fig. 7 MFM images show the domain configuration of the device consisting of two broad and one narrow high aspect ratio Py electrodes of 50 nm thickness and spaced by 200 nm in the region of the contact area (Fig. 1). While for the broad electrodes lateral kinks are included, they are omitted for the narrow electrode. All three electrodes approach the FM-SC contact window via inclined planes of the etched 200 nm thick sputtered Si-oxide which are depicted in the following as vertical flanks. We find an upper bound for the inclination angle of 55 degree for thermally grown and subsequently wet-etched 200 nm thick SiO_2 from cross-sectional scanning electron micrographs. Therefrom the

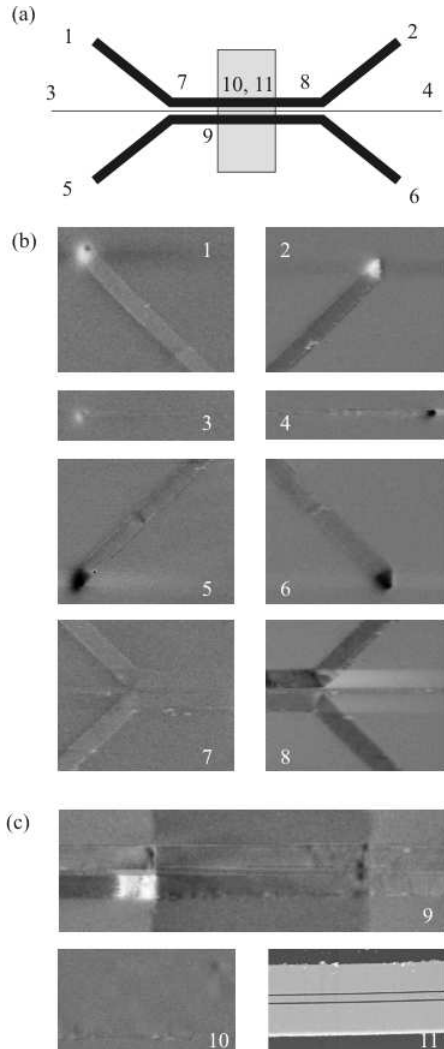


FIG. 7: MFM images of a lateral Py/InAs/Py device configuration consisting of two broad and one narrow high aspect ratio Py electrodes of 50 nm thickness, separated by 200 nm in the region of the contact area. (a) schematic view of the complete structure, 150 μm in length, with section numbering of MFM images displayed in (b) and (c). (b) Common stray field contrast at the ends of the broad wires (images 1,2,5,6) result from a multidomain configuration which originates from lateral kinks (images 7 and 8). The pair of strong black/white contrasts at the closures of the narrow wire (images 3 and 4) signals a single domain magnetization configuration. (c) Region of interest: FM-SC contact area. Stray field contrasts at the edges demonstrate domain wall pinning at vertical flanks (image 9) while the inner region shows no MFM contrasts (image 10, topography given in image 11).

lateral extension of the vertical flank amounts to about 140 nm. The narrow electrode has an overall aspect ratio of 375 ($l = 150 \mu\text{m}$, $w = 0.4 \mu\text{m}$) and steep flanks, which lead to the 20 μm long FM-SC contact area. Despite the steep flanks which could act as pinning centres for domain walls, only black and white contrasts (Fig. 7 (4),(5)) at the ends of the wire are visible, concluding

that this wire is in a single-domain state in remanence. In consequence, vertical flanks do not impose a multidomain state with domain walls in high aspect ratio wires. Contrary, the domain configuration of high aspect ratio electrodes with lateral kinks is more complex. Here, we investigate broad electrodes ($l = 145 \mu\text{m}$, $w = 2 \mu\text{m}$, i.e. high aspect ratio of 73) which are composed of several parts: the wire ends which are connected to the long mid-part by a lateral kink angle of 45° , and the long mid-part consisting of three $20 \mu\text{m}$ long wire sections (medium aspect ratios of 10, c.f. Fig. 1 and Fig. 7). The length from the wire end to its kink amounts $42 \mu\text{m}$ (high aspect ratio of 21). MFM images of these wire sections are depicted in Fig. 7 (b) by images 1, 2, 5 and 6, which show a uniform magnetization parallel to the length of the wire section and stray field contrasts at its end. However, at the lateral kink either a magnetization inhomogeneity (Fig. 7 (b) 1, 5) or a domain wall occurs (Fig. 7 (b) 2, 6). A uniform magnetization exists also in the section between the lateral kink and the steep flank leading to the FM-SC contact area (Fig. 7 (b) 1, 5). In Fig. 7 (c) the decisive section of the FM-SC contact area is displayed. Here, one can see the purpose of the steep flanks: they may pin domain walls outside the contact area so that the electrodes are uniformly magnetized along the FM-SC contact. A domain wall pinning leads to stray fields at the flanks as it is illustrated in Fig. 7 (c) by image 9. The existence of perpendicular stray field components may induce local Hall voltages in the semiconductor [5] and complicate the study of spin-dependent transport in lateral semiconductor-based spin-valve devices. For tunneling transport, however, as sought in FM-oxide-SC structures the impact of fringe fields at vertical flanks is regarded negligible by virtue of an exponentially decreasing tunneling current with increasing barrier (oxide) thickness. Furthermore, for the electrodes of different widths the FM-SC contact of the narrow electrode dominates the overall magnetoresistance which is designed without lateral kinks in the device layout discussed. In general, any remaining contribution to magnetoresistance on behalf of fringe fields can be characterized and circumvented by measurements in different four-terminal geometries. For a spin polarizing or detection electrodes uniform magnetization is a prerequisite which is accomplished by the wire sections of interest. In Fig. 7 (c), image 10 a MFM scan within the contact window strongly suggests uniform remanent magnetization along the FM-SC contact for all three electrodes. The slight magnetic contrasts visible are due to lift-off edges with a roughness less than the wire thickness ($\leq 30 \text{ nm}$). For comparison a topographic image of the contact area is shown in image 11. In summary, it was shown that introducing lateral kinks in high aspect ratio Py wires destroys a uniform magnetization configuration and may lead to formation of domain walls - highly undesirable in FM-SC devices. Steep flanks, however, can help maintaining a uniform magnetization configuration in the region of interest, here the FM-SC contact, by pinning of domain walls outside the

contact area. Vertical flanks, instead, prove harmless for the single domain behaviour of high aspect ratio electrodes.

IV. CONCLUSION

The optimization of the domain configuration of Py electrodes in a lateral hybrid device structure is presented. From the multidomain to single-domain transition it follows that for aspect ratios from $m \approx 4$ to $m \approx 20$ highly remanent states with closure domains exist, while for $m \gtrsim 20$ single-domain stray field contrasts are observed. Via magnetic field supported MFM we demonstrate the subsequent switching from parallel to antiparallel magnetization alignment of adjacent Py wires of varying widths as required for spin-valve operation. Lateral kink angles in low and high aspect ratio Py wires disturb the requested single domain state, while vertical flanks help to trap domain walls outside the ferromagnet-semiconductor contact. High aspect ratio electrodes at the FM-SC contact provide a single domain state in remanence essential for low- and zero-field operation.

Acknowledgments

The authors are grateful to M.-K. Sostarich for fruitful discussions. One of us (T. Last) gratefully acknowledges financial support by the Evangelisches Studienwerk Haus Villigst e.V. This work has been supported by the Deutsche Forschungsgemeinschaft within the Sonderforschungsbereich 491.

[1] S. Datta, B. Das, *Appl. Phys. Lett.* **56**, 665 (1990).

[2] G. Prinz, *Physics Today*, **48**, 58 (1995).

[3] for a review: D.D. Awschalom, D. Loss, N. Samarth (Eds), *Semiconductor Spintronics and Quantum Computation*, Springer, Berlin 2002.

[4] S. Hacia, T. Last, S.F. Fischer, U. Kunze, *J. of Superconductivity*, **16**, 1, 187 (2003).

[5] F.G. Monzon, M.L. Roukes, *J. Magn. Magn. Mat.*, **198**, 632 (1999).

[6] G. Meier, M. Halverscheid, T. Matsuyama, U. Merkt, *J. Appl. Phys.*, **89**, 7469 (2001).

[7] W. Rave, A. Hubert, *IEEE Transactions on magnetics*, **36**, 3886 (2000).

[8] A. Aharoni, *J. Appl. Phys.*, **63**, 5879 (1988).

[9] E. Seynaeve, G. Rens, A.V. Volodin, K. Temst, C. Van Haesendonck, Y. Bruynsraede, *J. Appl. Phys.* **89**, 531 (2001).

[10] T. Last, S. Hacia, S.F. Fischer, U. Kunze, *J. Magn. Magn. Mat.*, in press.

[11] J. Luo, H. Munekata, F.F. Fang, P.J. Stiles, *Phys. Rev. B*, **41**, 7685 (1990).

[12] E.A. de Andrade e Silva, G.C. La Rocca, F. Bassani, *Phys. Rev. B*, **55**, 16293 (1997).

[13] R.D. Gomez, T.V. Luu, A.O. Pak, K.J. Kirk, J.N. Chapman, *J. Appl. Phys.*, **85**, 6163 (1999).

[14] A. Hubert, R. Schäfer, *Magnetic Domains - The Analysis of Magnetic Microstructures*, Springer, Berlin 1998.

[15] R. Hertel, H. Kronmüller, *Phys. Rev. B* **66**, 7366 (1999).

[16] R.P. Cowburn, D.A. Allwood, G. Xiong, M.D. Cooke, *J. Appl. Phys.* **91**, 6949 (2002).